Approximate Transmission-Line Model for Field-to-Wire Coupling in Arbitrarily-Routed Wiring Structures Above Ground

Xiaokang Liu, *Member, IEEE,* Flavia Grassi, *Senior Member, IEEE,* Giordano Spadacini, *Senior Member, IEEE,* and Sergio A. Pignari, *Fellow, IEEE*

***Abstract*—In this article, a comprehensive method for parametric representation of wire trajectories, allowing accurate geometric description of complex and arbitrarily oriented wire bundles, is introduced. This is the starting point to develop a computationally efficient numerical transmission-line (TL) model for predicting the radiated susceptibility of arbitrarily oriented bundles of wires, illuminated by (possibly) nonuniform electromagnetic fields. The proposed method foresees solution of the field-to-wire coupling problem through suitable discretization and sampling of the bundle geometry and the incident electromagnetic field. Differently from previous models, where bundles parallel to ground were assumed, the proposed model allows for arbitrary bundle orientation by exploiting, first, exact projection of the external field onto the bundle direction, and second, evaluation of the actual wire length (instead of the longitudinal one) of each TL section. Accuracy and computational efficiency of the proposed method are assessed versus full-wave simulation for two application examples, involving parabola-shaped and trefoil knot-shaped wiring structures above ground. Although the strong nonuniformity affecting these structures forces TL theory to work very close to its limits, the achieved agreement is satisfactory and the significant reduction of computational times makes the proposed method suitable for approximate yet efficient prediction of radiated susceptibility characteristics of complex wire bundles.**

***Index Terms*—Field-to-wire coupling, multiconductor transmission-line (MTL), nonuniform transmission lines, radiated susceptibility (RS), random wire bundles.**

I. Introduction

Complex hand-assembled cable geometries are widely exploited in several industrial sectors, e.g., in aerospace and automotive systems. Due to the overall complexity of the system where several data and power lines coexist in close proximity, assuring the immunity of the whole system is a critical task, since cables can quite efficiently pick up external interference and convey it to the terminal units [1]. Hence, starting from the early design stage, the availability of radiated susceptibility (RS) prediction models can provide the designer with essential information on the possible system-level noise so to plan in advance suitable mitigation strategies assuring system reliability (e.g., by optimization of the cable routing).

State-of-the-art approaches to investigate field-to-wire coupling [2] involve full-wave numerical simulation, assuring accurate prediction at the cost of quite long simulation times, as well as techniques based on transmission-line (TL) theory, which have the potential to provide a more computationally efficient solution, by exploiting suitable simplifying assumptions. For cables installed in large and complex electromagnetic (EM) environments, hybrid approaches have been developed to mitigate the excessive computational burden of full-wave simulations [1], [3]–[5]. According to these approaches, the nonuniform field impinging the bundle under analysis is numerically evaluated (in the absence of the cable) by full-wave simulation at discrete positions along the cable path. The obtained field samples are then combined with a computational efficient TL-based model of the wiring structure, regarded as the cascade connection of approximately uniform line sections (so called uniform cascade section method [6]) with induced sources at the terminations evaluated by exploiting the field samples numerically calculated.

In spite of bundle complexity, these approaches are proven to provide accurate prediction of the noise induced at the terminal sections on condition that the cable axis is approximately parallel to ground. Conversely, they suffer from a significant lack of accuracy in case of wiring harnesses exhibiting pronounced nonuniformity with respect to ground, as often occurs in practical installations. Approaches based on the so-called *TL super theory* [7], [8] can overcome this limitation, but they are quite complex and not so computationally efficient [9]. As an alternative solution, a modeling method based on modal decomposition was developed in [9]. However, since common-mode components are anyway modelled by the method of moments (MoM), the method still suffers from low computational efficiency.

This work contributes to the prediction of EM interference in complex wiring harnesses, by developing an approximate yet accurate numerical TL-based approach no longer constrained by the preliminary assumptions limiting the applicability of previous models. Namely, the wiring bundles here considered are arbitrarily oriented and strongly nonuniform, with the twofold consequence that: first, they cannot be longer regarded as approximately parallel to ground, and second, basic assumptions of TL theory, such as for instance $h \ll \lambda$ (where h denotes the wire height above ground, and λ is the wavelength), may be locally violated or only partially satisfied.

To this end, a general mathematical framework, based on the Frenet frame [10], is introduced to provide the harness under analysis with a suitable parametric representation. A semianalytical model is firstly introduced, which is based on the classical Agrawal model [11] applied to the aforesaid mathematical representation of wire trajectories. This method, here used as the reference to assess the accuracy of exact

TL-based approaches, can assure accurate prediction of the induced interference on condition that analytical expressions are available not only for the wire trajectories, but also for the external field. Moreover, it is usually prohibitive in terms of computational time.

Although approximate, the numerical model here proposed can assure comparable prediction accuracy. However, it outperforms the semianalytical approach not only in terms of computational efficiency, but also in terms of flexibility in the acceptable input data. As a matter of fact, it can be efficiently applied even when the external field and the wire trajectories are only known at discrete points along the cable path.

Suitable examples involving wiring structures exhibiting strong nonuniformity with respect to ground are presented in order to prove the effectiveness of the proposed numerical model. Despite the basic assumptions of TL theory are barely satisfied, in most of the examples the maximum observed discrepancies with respect to fullwave simulation are in the order of a few decibels only.

The rest of this article is organized as follows. Section II introduces the mathematical framework for parametric representation of complex bundle geometries. Starting from such a mathematical representation, in Section III, a semianalytical RS model is firstly derived, followed by the development of the approximate numerical RS model here proposed. Performance of the proposed method w.r.t. full-wave simulation and semianalytical TL-based prediction is investigated in Sections IV and V by suitable test cases, involving parabola-shaped and knot-shaped wiring structures, respectively. Finally, Section VI concludes this article.

II. Parametric Representation of Complex Bundle Geometries

This Section introduces a general framework for parametric representation of complex wiring harnesses. To this end, the geometry of the cable bundle under analysis is modeled by its center trajectory in terms of parametric curve in a 3-D Euclidean space. For instance, by introducing the independent variable u, the trajectory of a wire in the bundle is represented by the curve $\mathbf{Q}(u) = [x(u), y(u), z(u)], u \in [U_{\text{lower}}, U_{\text{upper}}]$, where $x(u)$, $y(u)$ and $z(u)$ denote the vertical, horizontal, and longitudinal coordinate functions in a right-handed orthonormal system, respectively (see Fig. 1). If the ground plane exists, it is usually located in the $(y-z)$ plane.

To model a bundle of wires starting from the reference path $\mathbf{Q}(u)$, a smoothly varying coordinate system needs to be adopted such that the perpendicular plane to the path is always well defined. To this end, the Frenet frame is adopted, which is a moving frame along a 3-D curve, characterized by orthogonal axis vectors [10]

$$\mathbf{t}(u) = \frac{\mathbf{Q}'(u)}{\|\mathbf{Q}'(u)\|} \tag{1}$$

$$\mathbf{b}(u) = \frac{\mathbf{Q}'(u) \times \mathbf{Q}''(u)}{\|\mathbf{Q}'(u) \times \mathbf{Q}''(u)\|} \tag{2}$$

$$\mathbf{n}(u) = \frac{\mathbf{b}(u) \times \mathbf{t}(u)}{\|\mathbf{b}(u) \times \mathbf{t}(u)\|} \tag{3}$$

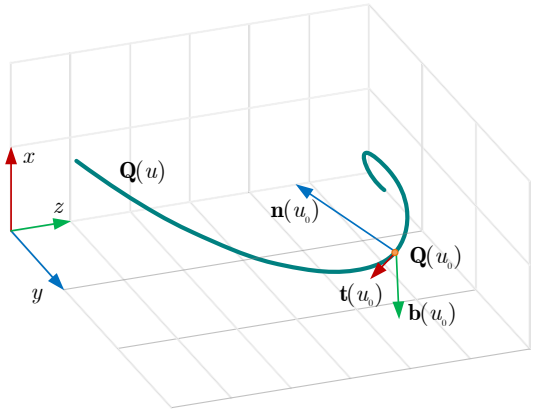

Fig. 1. Illustration of a 3-D wire trajectory $\mathbf{Q}(u)$ in Euclidean frame and Frenet frame vectors at $\mathbf{Q}(u_0)$.

where $\mathbf{t}(u)$ is the normalized tangent vector, $\mathbf{b}(u)$ is the normalized binormal vector, and $\mathbf{n}(u)$ is the normalized normal vector. Accordingly, the trajectory $\mathbf{Q}_n(u)$ of the nth wire in the bundle is represented as the combination of the reference path $\mathbf{Q}(u)$ and its pertinent offset in the orthonormal plane as

$$\mathbf{Q}_n(u) = \mathbf{Q}(u) + \kappa_{1,n}(u)\mathbf{n}(u) + \kappa_{2,n}(u)\mathbf{b}(u). \tag{4}$$

By means of (4), bundles comprising N parallel wires can be generated by enforcing invariant relative wire positions, more complex wiring structures by properly selecting suitable contour-related functions $\kappa_{1,n}(u)$ and $\kappa_{2,n}(u)$.

Although this work will mainly focus on the modelling of arbitrary cable routing (and, hence, the presented examples will involve a minimum number of wires only), it is worth noticing that the geometrical representation in (4) is rather general and can be easily exploited for the modeling of complex wire bundles possibly exhibiting arbitrary cross sections. Such an extension of the model proposed in this work can be achieved by combining it with the methodology introduced in [5], which allows accounting for random movements of the wires along the cable length.

III. RS Model

Aim of this section is to derive a TL-based RS model, characterized by wide applicability, high accuracy and moderate computational burden, for the prediction of noise voltage/currents induced by a nonuniform EM field at the terminations of an arbitrarily oriented wire bundle running above ground. To this end, a semianalytical RS model is firstly presented, whose limitations are afterward overcome by a simplified yet accurate and more computationally efficient numerical model.

A. Semianalytical Solution

According to TL theory, the $N \times 1$ vectors of voltages $(\mathbf{V}_{\text{L}}, \mathbf{V}_{\text{R}})$ and currents $(\mathbf{I}_{\text{L}}, \mathbf{I}_{\text{R}})$ induced at the terminal ends of a N-wire bundle illuminated by an external EM field are computed by resorting to the schematic representation in Fig.

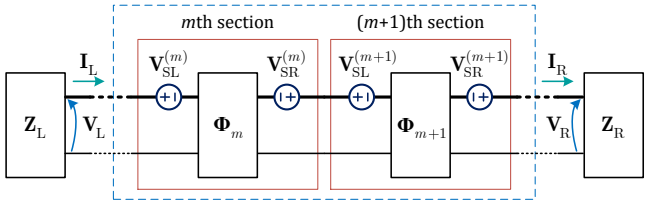

Fig. 2. MTL modeling of the general wire bundle for computation of the terminal response. The thick line represents N wires and the thin line represents the ground.

2. The wire bundle, modelled as a nonuniform multiconductor TL (MTL), is subdivided into M sections with approximately uniform cross section, and characterized by suitable chain-parameter matrices $\mathbf{\Phi}_1, \ldots, \mathbf{\Phi}_M$ with expression

$$\mathbf{\Phi}_m = \begin{bmatrix} \cos\left(\beta_0 \bar{\mathscr{L}}_m\right) \mathbf{1}_{N\times N} & -j\mathbf{Z_C} \sin\left(\beta_0 \bar{\mathscr{L}}_m\right) \\ -j\mathbf{Z_C}^{-1} \sin\left(\beta_0 \bar{\mathscr{L}}_m\right) & \cos\left(\beta_0 \bar{\mathscr{L}}_m\right) \mathbf{1}_{N\times N} \end{bmatrix} \tag{5}$$

where $\mathbf{Z_C} = c_0\mathbf{L}$ is the $N\times N$ characteristic impedance matrix (c_0 being the speed of light in free space and $\mathbf{L}$ being the p.u.l. inductance matrix), $\beta_0 = \omega/c_0$, ω is the angular frequency, $\bar{\mathscr{L}}_m$ is the average actual wire length of section m, and $\mathbf{1}_{N\times N}$ is the $N \times N$ identity matrix.

In this representation, the actual wire lengths of different conductors belonging to the mth section are assumed to be approximately identical. However, the resulting average length of a specific section can be even significantly different from its axial length.

Effects due to the impinging field are included by means of lumped voltage sources ($\mathbf{V}_{\text{SL}}$, $\mathbf{V}_{\text{SR}}$) connected by the sides of each line section, and evaluated according to the Agrawal field-to-wire coupling model in [11]. Line solution is achieved by enforcing at the line ends the port constraints due to the terminal loads (matrices $\mathbf{Z}_{\text{L}}$, $\mathbf{Z}_{\text{R}}$).

For wiring harnesses with complex and highly non uniform geometry, two aspects of the evaluation of the chain-parameter matrices associated with each line section are worth to be mentioned. First, the actual wire length, instead of the longitudinal section length, is to be considered. Second, the p.u.l. parameters of each line section need to be evaluated by considering the cross section perpendicular to the ground plane. Since in a specific cross section, wire positions are identified by different values of u, determining the actual wire positions requires numerical solution of nonlinear equations, cast by imposing the wire longitudinal coordinate constraint and considering the pertinent parameter range.

Without loss of generality, let us consider the mth MTL section, with common longitudinal coordinate bounded by $z \in [z_{\text{BL}}, z_{\text{BR}}]$ [the superscript (m) is hereinafter omitted for brevity], and lower and upper parameter range given by

$$\mathbf{U}_X = [U_{X,1}, u_{X,2}, \ldots, U_{X,N}], \;\; X = \text{L}, \text{R} \tag{6}$$

If the Agrawal formulation in [11] is adopted in combination with the p.u.l. parameter matrices, the description of field coupling onto the wires can be obtained as in [12], [13], incorporating vectors of the scattered voltages and currents. By solution of this representation, analytical expressions for the induced terminal sources accounting for field-to-wire coupling effects are obtained (more details on the derivation can be found in [12]).

Specifically, for the nth wire with trajectory $\mathbf{Q}_n(u) = [x_n(u), y_n(u), z_n(u)]$, where $u \in [U_{\text{L},n}, U_{\text{R},n}]$, the equivalent lumped voltage sources induced by the external field are cast as the sum of two contributions as [13]

$$V_{\text{S}X,n} = V^{(l)}_{\text{S}X,n} + V^{(v)}_{\text{S}X,n}, \;\; X = \text{L}, \text{R} \tag{7}$$

the former, superscript (l), due to the longitudinal field component, the latter, superscript (v), due to the vertical one [1], [13]. The generators due to the longitudinal contribution take different expressions at the left and right ends, whereas the expression of the generators due to the vertical contribution is the same at both ends. Specifically, those due to the longitudinal component are calculated as

$$\begin{aligned} V^{(l)}_{\text{SL},n} &= \int_{\mathcal{C}_n} \frac{\sin\left[\beta_0\left(\ell_n - \mathscr{L}_n\right)\right]}{\sin\left(\beta_0 \mathscr{L}_n\right)} \left[\mathbf{E}\left(\mathbf{Q}_n\right) \cdot \mathbf{l}_n\right] d\ell_n \\ V^{(l)}_{\text{SR},n} &= \int_{\mathcal{C}_n} \frac{\sin\left(\beta_0 \ell_n\right)}{\sin\left(\beta_0 \mathscr{L}_n\right)} \left[\mathbf{E}\left(\mathbf{Q}_n\right) \cdot \mathbf{l}_n\right] d\ell_n \end{aligned} \tag{8}$$

where $\ell_n(u)$ is the curvilinear abscissa starting from $\mathbf{Q}_n(U_{\text{L},n})$, i.e. $\ell_n(u) = \int_{U_{\text{L},n}}^{u} d\ell_n(u)$; $\mathscr{L}_n$ is the actual length of wire n within section m, i.e., $\mathscr{L}_n = \ell_n(U_{\text{R},n})$; $\mathbf{l}_n = \frac{d\mathbf{Q}_n/d\ell_n}{\|d\mathbf{Q}_n/d\ell_n\|} = \frac{d\mathbf{Q}_n/du}{\|d\mathbf{Q}_n/du\|}$ is the unit direction vector function; $\mathcal{C}_n$ is the curvilinear path of the line integral in the pertinent section. Eventually, $\mathbf{E}\left(\mathbf{Q}_n\right) = \left[E_x\left(\mathbf{Q}_n\right), E_y\left(\mathbf{Q}_n\right), E_z\left(\mathbf{Q}_n\right)\right]$ denotes the vector of the incident electric field, which is assumed to be continuously defined and known in $u \in [U_{\text{L},n}, U_{\text{R},n}]$. Hence, by introducing

$$g_n(u) = \sqrt{\left(\frac{dx_n(u)}{du}\right)^2 + \left(\frac{dy_n(u)}{du}\right)^2 + \left(\frac{dz_n(u)}{du}\right)^2} \tag{9}$$

the infinitesimal curvilinear abscissa $d\ell_n$ is expressed as $d\ell_n(u) = g_n(u)\, du$, and the expressions in (8) are accordingly reformulated as

$$\begin{aligned} V^{(l)}_{\text{SL},n} &= \int_{U_{\text{L},n}}^{U_{\text{R},n}} \frac{\sin\left[\beta_0\left(\ell_n - \mathscr{L}_n\right)\right]}{\sin\left(\beta_0 \mathscr{L}_n\right)} \left[\mathbf{E}\left(\mathbf{Q}_n\right) \cdot \mathbf{l}_n\right] g_n(u)\, du \\ V^{(l)}_{\text{SR},n} &= \int_{U_{\text{L},n}}^{U_{\text{R},n}} \frac{\sin\left(\beta_0 \ell_n\right)}{\sin\left(\beta_0 \mathscr{L}_n\right)} \left[\mathbf{E}\left(\mathbf{Q}_n\right) \cdot \mathbf{l}_n\right] g_n(u)\, du. \end{aligned} \tag{10}$$

Conversely, the generators due to the vertical component take the expression

$$V^{(v)}_{\text{S}X,n} = -\int_0^{x_n(U_{X,n})} E_x\left(x, y_n\left(U_{X,n}\right), z_n\left(U_{X,n}\right)\right) dx \tag{11}$$

where $X = \text{L}, \text{R}$ denotes the left and right termination.

If the analytic expression of the incident field $\mathbf{E}\left(\mathbf{Q}_n\right)$ is available for every wire inside the bundle, the integrals in (10) and (11) in some specific cases can be evaluated analytically.

In general, they can be computed by resorting to numerical integration methods.

B. Numerical RS Model

The solution approach presented in the previous section provides accurate prediction of the noise induced at the terminal sections of the bundle under analysis. However, it generally requires significantly large computational times, mainly due to the numerical solution of the integrals in (10) and (11). Moreover, since it requires a continuous representation of the wire trajectories and of the incident field, it can be actually applied on condition that the bundle geometry and the characteristics of the incident field are quite canonical. For instance, it is not applicable if the wire geometry and/or the incident field are known in terms of discrete series of samples.

To overcome these limitations, approximate yet efficient field-to-wire coupling models involving wire/TWP bundles exhibiting deterministic [1] and random [3] cross sections have been previously developed and validated. These models assume that the bundle axis is approximately parallel to the ground plane and evaluate to drastically simplify the evaluation of the generators due to the longitudinal field contribution by means of suitable approximations. In these models, the bundle axis is assumed to be approximately parallel to the ground plane, thus resulting in approximate values of the longitudinal field contribution. The aforesaid assumption limits the applicability of the models in [1] and [3] to well-controlled cable layouts.

The numerical method presented in this section aims at overcoming the aforesaid limitation, in order to allow interference prediction in complex wire bundles with arbitrary local orientation with respect to ground. Likewise the methods in [1] and [3], the preliminary assumption is that the incident field and the wire geometry are known by samples and linearly interpolated along the bundle axis. However, the following hold.

1) To evaluate the induced generators due to the longitudinal contribution, the wires are considered to be arbitrarily directed, straight, short line segments not necessarily parallel to the longitudinal axis (z-axis).
2) To evaluate the induced generators due to the vertical field component, different heights are considered at the ends of each wire segment instead of constant height above ground.
3) To evaluate the induced sources and the chain-parameter matrices in Fig. 2, the actual wire length is considered in each MTL section instead of its projection in the longitudinal projection.

To this end, the incident electric field quantities at the ends of the mth section and for the nth wire (i.e., evaluated at $u = U_{\mathrm{L},n}$ and $u = U_{\mathrm{R},n}$) are sampled as the real parts $E_{k,\mathrm{RE}}\left(\mathbf{Q}_n\left(u\right)\right)$ $(k = x, y, z)$ and the imaginary parts $E_{k,\mathrm{IM}}\left(\mathbf{Q}_n\left(u\right)\right)$ of the vertical/horizontal/longitudinal components.

According to Spadacini *et al*. [1], the first step for the derivation of the proposed numerical model foresees linear interpolation of the field samples along $\mathbf{Q}_n$ (with $u \in [U_{\mathrm{L},n}, U_{\mathrm{R},n}]$) in the three directions. This yields

$$\begin{aligned}\mathbf{E}\left(\mathbf{Q}_n\right) \cong & \left[\left(a_x x + b_x\right) + j\left(c_x x + d_x\right)\right]\vec{a}_x \\ & + \left[\left(a_y y + b_y\right) + j\left(c_y y + d_y\right)\right]\vec{a}_y \\ & + \left[\left(a_z z + b_z\right) + j\left(c_z z + d_z\right)\right]\vec{a}_z\end{aligned} \tag{12}$$

where $\vec{a}_x$, $\vec{a}_y$, and $\vec{a}_z$ are the unit vectors of the Cartesian coordinate system, and

$$\begin{aligned}a_k &= \left[E_{k,\mathrm{RE}}\left(\mathbf{Q}_n\left(U_{\mathrm{R},n}\right)\right) - E_{k,\mathrm{RE}}\left(\mathbf{Q}_n\left(U_{\mathrm{L},n}\right)\right)\right]/\mathscr{L}_n \\ b_k &= E_{k,\mathrm{RE}}\left(\mathbf{Q}_n\left(U_{\mathrm{L},n}\right)\right) \\ c_k &= \left[E_{k,\mathrm{IM}}\left(\mathbf{Q}_n\left(U_{\mathrm{R},n}\right)\right) - E_{k,\mathrm{IM}}\left(\mathbf{Q}_n\left(U_{\mathrm{L},n}\right)\right)\right]/\mathscr{L}_n \\ d_k &= E_{k,\mathrm{IM}}\left(\mathbf{Q}_n\left(U_{\mathrm{L},n}\right)\right)\end{aligned} \tag{13}$$

Besides, for the nth wire, the unit-direction vector function in the pertinent range is approximated as

$$\begin{aligned}\mathbf{l}_n &\cong \left[x_n\left(U_{\mathrm{R},n}\right) - x_n\left(U_{\mathrm{L},n}\right)\right]/\mathscr{L}_n \cdot \vec{a}_x \\ &\quad + \left[y_n\left(U_{\mathrm{R},n}\right) - y_n\left(U_{\mathrm{L},n}\right)\right]/\mathscr{L}_n \cdot \vec{a}_y \\ &\quad + \left[z_n\left(U_{\mathrm{R},n}\right) - z_n\left(U_{\mathrm{L},n}\right)\right]/\mathscr{L}_n \cdot \vec{a}_z \\ &\triangleq \left[\xi_x, \xi_y, \xi_z\right]\end{aligned} \tag{14}$$

By substituting (12)-(14) into (8) and (11), the induced sources associated with the longitudinal and vertical field components in (7) are obtained. Particularly, the sources associated with the longitudinal field contribution are written as sum of three-dimensional components as

$$V^{(l)}_{\mathrm{S}X,n} = \sum_{k=x,y,z} \xi_k\left[\left(a_k + jc_k\right)\Sigma_X + \left(b_k + jd_k\right)\Psi_X\right] \tag{15}$$

where $X = \mathrm{L}, \mathrm{R}$, and

$$\Sigma_{\mathrm{L}} = \frac{\sin\left(\beta_0\mathscr{L}_n\right) - \beta_0\mathscr{L}_n}{\beta_0^2\sin\left(\beta_0\mathscr{L}_n\right)} \tag{16}$$

$$\Sigma_{\mathrm{R}} = \frac{\sin\left(\beta_0\mathscr{L}_n\right) - \beta_0\mathscr{L}_n\cos\left(\beta_0\mathscr{L}_n\right)}{\beta_0^2\sin\left(\beta_0\mathscr{L}_n\right)} \tag{17}$$

$$\Psi_{\substack{\mathrm{L}\\\mathrm{R}}} = \pm\frac{\cos\left(\beta_0\mathscr{L}_n\right) - 1}{\beta_0\sin\left(\beta_0\mathscr{L}_n\right)}. \tag{18}$$

Conversely, the sources associated with the vertical field contribution are calculated by considering x-direction components only. This yields

$$\begin{aligned}V^{(v)}_{\mathrm{S}X,n} = & -\left[E_{x,\mathrm{RE}}\left(\mathbf{Q}_n\left(U_{X,n}\right)\right) + jE_{x,\mathrm{IM}}\left(\mathbf{Q}_n\left(U_{X,n}\right)\right)\right] \\ & \cdot x_n\left(U_{X,n}\right).\end{aligned} \tag{19}$$

Once the distributed voltage sources are determined, prediction of the voltages/currents at the ends of the bundle is obtained by solving the model in Fig. 2. Accuracy and computational efficiency of this numerical model will be assessed in the following Sections, where wiring structures not satisfying the assumptions in [1] and [3] will be considered.

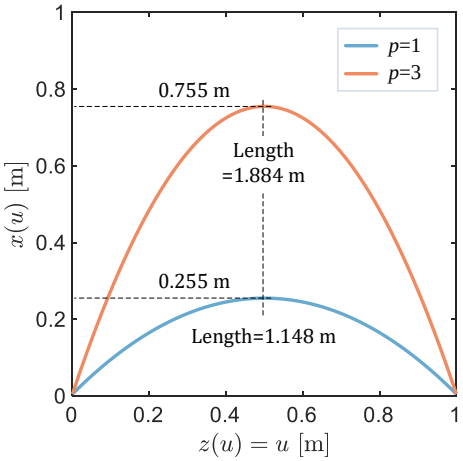

Fig. 3. Parabola-shaped TLs under analysis: Projection on the $(x-z)$ plane (at $y=0$).

IV. Example I: Parabola-Shaped Wiring Structures

In this Section, the proposed RS model is applied to a parabola-shaped TL above ground. Two examples with different degree of curvature are considered in order to investigate the impact of different nonuniformity with respect to ground. Accuracy and computational effectiveness of the proposed numerical model are assessed by comparison versus predictions obtained by the semianalytical model in Section III-A and by full-wave (MoM) simulation.

A. Geometric Description

For the sake of simplicity, the trajectory of the line conductor is located in the $(x-z)$ plane, with axial length $L=1$ m and longitudinal coordinate from $z=0$ to $z=L$. The wire trajectory can be written as

$$\begin{cases} x(u) = -p(u-0.5L)^2 + 0.25pL^2 + h_0 \\ y(u) = 0 \\ z(u) = u \end{cases} \tag{20}$$

where $h_0 = 5$ mm denotes the initial height above ground at the line ends, and p is a coefficient controlling the degree of curvature. Two cases, i.e., $p=1$ and $p=3$ (see Fig. 3), are studied. It is worth noticing that for $p=3$ the structure exhibits significant nonuniformity, with the actual wire length (1.884 m) being approximately twice the longitudinal length (1 m).

B. Prediction of the Terminal Voltages

In both cases, a bare wire with radius of 0.25 mm is considered. Effects due to the vertical risers [14], [15] (i.e., the wire segments connecting the wire ends to ground) are here disregarded due to the negligible height of the wire terminal sections. At both ends, the wire is connected to ground by an impedance $Z = 150\ \Omega$. To provide well-controlled test cases for assessing model validity, the EM field impinging the line is modelled as a plane-wave field. Without loss of generality,

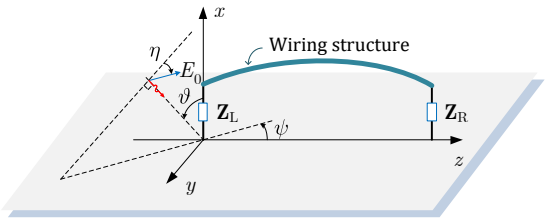

Fig. 4. Parameters of the incident plane-wave field. The parabola-shaped wiring structure is terminated to ground through equivalent Thevenin impedance matrices at both ends.

this choice allows evaluating the electric field samples to be input in the proposed MTL model by closed-form solution of Maxwell equations [6], thus avoiding possible issues related to numerical evaluation of the incident field. General incidence conditions are assumed for the uniform plane-wave field impinging upon the line. With reference to Fig. 4, a plane wave with electric field strength $E_0 = 1$ V/m, elevation angle $\vartheta = 50°$, azimuth angle $\psi = 20°$, and polarization angle $\eta = 60°$ is considered.

For calculation, the wire was evenly subdivided into 400 sections along the axial length, and pertinent per-unit-length parameters were evaluated for each line section. The exploited number of sections was selected as a tradeoff between accuracy and computational efficiency, as it assured a maximum error below 1% (iterative procedure with respect to the number of sections) in the prediction of terminal voltages by the MTL-based RS model. Examples of the obtained results are shown in Fig. 5, where predictions of the voltage induced at the left TL end are compared. Despite the wiring structures under analysis do not satisfy basic TL theory assumptions (especially for p=3), a satisfactory agreement between the predictions obtained by the two TL-based methods (blue and red curves) and full-wave MoM simulation (green curves) can be appreciated in the overall frequency interval from 100 kHz up to 2 GHz. The result is particularly interesting for p=3, where only slight discrepancies between TL solutions and full-wave simulation are observed for frequencies up to 500 MHz. At higher frequencies, where $h/\lambda > 1/3$, the differences gradually increase due to phenomena that cannot be predicted by TL theory (e.g., higher-order propagation modes, re-radiation losses). Consistently, the predictions obtained by the proposed numerical method and the semianalytical solution are coincident in the whole frequency interval up to 2 GHz. However, they significantly differ in terms of computational times, as discussed in the next section.

C. Computational Efficiency

In the previous examples, terminal voltages were calculated at 431 discrete frequency points (i.e., 100 logarithmically spaced points per decade) in the interval from 100 kHz up to 2 GHz. All simulations were performed on a standard desktop PC with an Intel(R) Core(TM) i5-7400 CPU running at 3.0 GHz and 16 GB of RAM. To accelerate the computation, parallel computing, exploiting the 4 processors of the multicore CPU, was used both for the MoM solver and for the semianalytic model (by the Parallel Computing Toolbox available

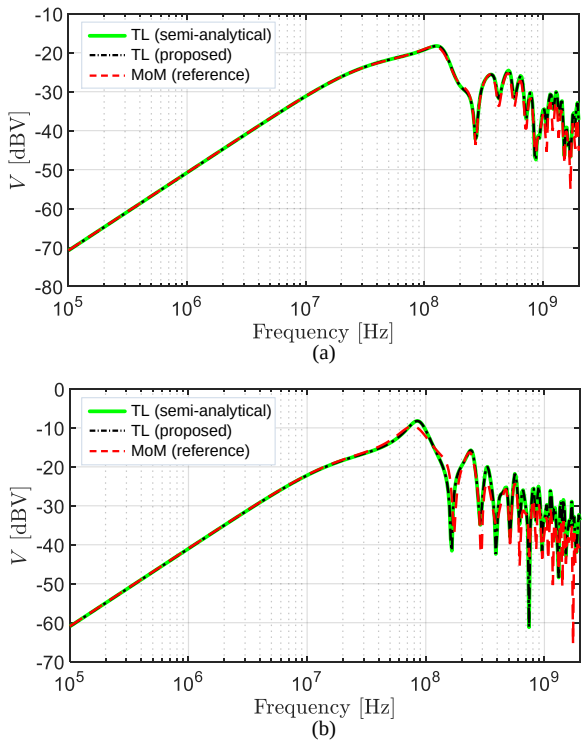

Fig. 5. Voltage induced at the left terminal of the parabola-shaped wire in Fig. 4: (a) $p = 1$; and (b) $p = 3$.

TABLE I
COMPUTATIONAL TIME

	MoM	semi-analytical	proposed
Parabola: $p = 1$	729.4 s	3769.6 s	5.8 s
Parabola: $p = 3$	1562.2 s	3943.4 s	
Reference knot	2555.9 s	24384.5 s	
Tight knot	1760.9 s	24088.9 s	14.0 s
Tall knot	3334.0 s	24202.3 s	

in MATLAB). For consistent comparison of the computational efficiency, where parallel computing was adopted, the sum of the CPU times of all the processors was calculated. The obtained computational times are collected in Table I. For TL-based methods, the listed times have to be increased by 3.1 s, which represents the time required to preliminary evaluate the p.u.l. parameters (by the method in [16]) for 400 line cross sections.

The comparison proves the effectiveness of the proposed technique, which allows for a drastic reduction of computational times w.r.t. the other techniques. Particularly, the time required for MoM-based simulations is strongly influenced by the curvilinear segmentation of the wiring structure. In the proposed examples, the number of required segments (using fine mesh size) increased from 194 segments for $p = 1$ to 316 segments for $p = 3$, with a proportional increase of the computational time which is nearly doubled in the second example. Conversely, since TL-based approaches adopt the same wire segmentation in both cases, the computational time for $p = 1$ and $p = 3$ is nearly the same. However, the prediction based on the semianalytic model is highly time-consuming, even w.r.t. full-wave simulation due to complexity and low efficiency in handling symbolic math in combination with numerical integration. Conversely, the proposed method allows very fast prediction in both cases.

V. EXAMPLE II: TREFOIL KNOT STRUCTURE

In this Section, the proposed method is applied to predict field coupling onto a more complex wiring structure involving a trefoil knot. While clearly in practical situations, cables do not exhibit knots, we consider the trefoil knot a trajectory suited to test the ability and robustness of TL theory to model highly nonuniform and complex wire shapes. Indeed, in a trefoil knot, TL-theory assumptions are pushed to the limits as the longitudinal coordinate is no longer monotonically increasing along the entire extension of the line, and EM interactions between neighbouring parts of the knot, not accounted for by the proposed model, are possible.

A. Geometric Description

To provide a geometric description of trefoil knot structures, several parametric representations, including trigonometric functions [17] and polynomial functions [18], can be found in the literature. Here, the polynomial notation is adopted, with suitable rotation and scaling as

$$\begin{cases} x(u) = -K_1 K_2 \left(u^4 - 4u^2\right) + h_0 \\ y(u) = K_1 K_3 K_4 \left(u^5 - 10u\right) \cos\theta - K_1 K_4 \left(u^3 - 3u\right) \sin\theta \\ z(u) = K_1 K_3 K_5 \left(u^5 - 10u\right) \sin\theta + K_1 K_5 \left(u^3 - 3u\right) \cos\theta \end{cases} \tag{21}$$

where K_i (i=1,..,5) are scaling factors; $h_0 = 5$ mm is the vertical offset and θ is the rotation angle. In the following examples, the reference wire trajectory is generated by assuming: $u \in [-2, 2]$, $K_1 = 0.1$, $K_3 = 0.2$, $h_0 = 5$ mm, and $\theta = 50°$. Two different values of K_2 are exploited, i.e., $K_2 = 0.5$ and $K_2 = 1$, to deform the knot in the vertical direction (the larger value corresponding to a taller knot). In a similar fashion, two different values of K_4 are used ($K_4 = 1$ and $K_4 = 3$) to deform the knot in the horizontal direction (the larger value corresponding to a larger knot), and two different values of K_5 are used ($K_5 = 0.5$ and $K_5 = 1$) to deform the knot in the longitudinal direction. 3-D pictures of the generated knot structures are shown in Fig. 6. The knot shown in the first panel was obtained by setting the previous coefficients to the values $K_2 = 0.5$, $K_4 = 3$, and $K_5 = 1$, respectively. Such a knot, characterized by a peak height of 0.205 m and total wire length of 2.221 m, will be referred to as *reference knot* in the following. The second knot is obtained from the previous one, by reducing the horizontal thickness (i.e., by setting $K_4 = 1$, with K_2 and K_5 constant to the original value). This can be appreciated in the second panel of Fig. 6, where the lateral view of the original knot (left) is compared with the one of the new knot (right). Such a knot, hereinafter denoted as *tight knot*, is characterized by peak height of 0.205 m and total wire length of 1.991 m. The third knot (hereinafter referred to as *tall knot*) is obtained from the reference one by increasing

TABLE II
KNOT CONFIGURATIONS UNDER ANALYSIS

Bundle	K_2	K_4	K_5	Peak height	Length
Reference knot	0.5	3	1	0.205 m	2.221 m
Tight knot	0.5	1	1	0.205 m	1.991 m
Tall knot	1	3	1	0.405 m	2.683 m
Small knot	0.5	3	0.5	0.205 m	1.590 m

the vertical deformation (i.e., by setting $K_2 = K_5 = 1$ and $K_4 = 3$). Such a knot exhibits peak height of 0.405 m and total wire length of 2.683 m. The front view of this knot is shown in Fig. 6(d). Eventually, a fourth knot [hereinafter referred to as *small knot*, as shown in 6(e)] is obtained from the reference one by decreasing its longitudinal size (i.e., by setting $K_2 = 0.5$, $K_4 = 3$, and $K_5 = 0.5$). The peak height is 0.205 m and total wire length is 1.590 m. Table II collects relevant characteristics of the four knots under analysis.

B. Single-Wire Knot: Prediction of Terminal Voltages

To predict the voltages induced at the terminations of single-wire knot geometries (i.e., the knot structures shown in Fig. 6), wire characteristics, terminal loads, and parameters of the incident plane-wave fields are set as in the previous examples. For TL modelling, pertinent p.u.l. parameters were evaluated for 1000 line cross sections, ignoring the presence of other segments belonging to the line trajectory and crossing the cross section of interest. Predictions of the voltage induced at the line left terminal, obtained by MoM-based and TL-based methods, are compared in Fig. 7. The required computation times are collected in Table I. For TL-based methods, the listed times should be increased by 7.7 s for evaluating the p.u.l. parameters by Clements *et al*. [16]. The comparison shows that both TL-based methods can assure the same prediction accuracy, as well as a general satisfactory agreement with the prediction obtained by full-wave simulation in the whole frequency interval up to 2 GHz. More specifically, TL-based predictions are in very good agreement with MoM solution for the *reference knot*, which is less critical w.r.t. to the *tall knot* in terms of height above ground, and less affected than the *tight knot* and *small knot* by near-field coupling between neighbouring sections. Prediction accuracy is still satisfactory also for the other three knots, even if the observed discrepancies slightly increase with frequency in the hundreds of megahertz range.

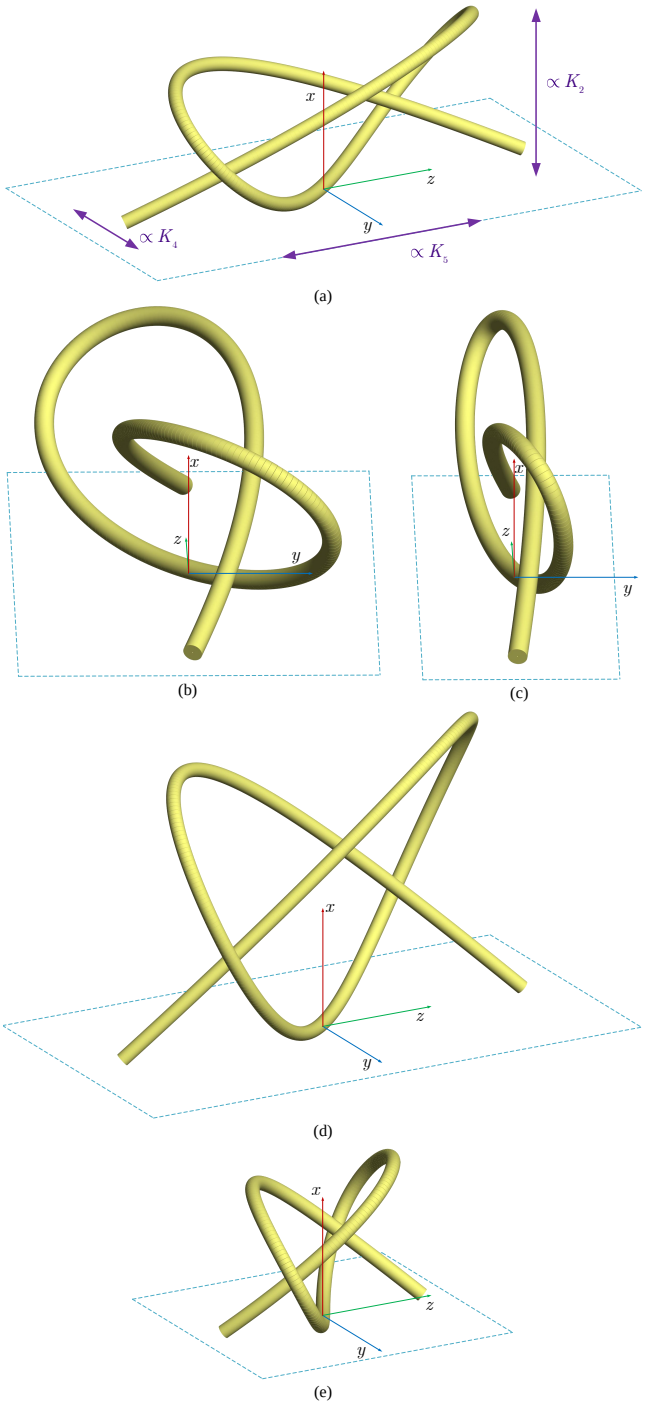

Fig. 6. Generated knot structures (reference trajectories). *Reference knot* with (a) front and (b) lateral views. (c) Lateral view of *tight knot*, (d) front view of *tall knot*, and (e) front view of *small knot*.

C. Knotted Wire-Pair: Prediction of Modal Voltages

To realize a knotted wire pair, an additional wire was generated running parallel to the original one (denoted as wire 1), by exploiting (4) with $\kappa_{1,2}(u) = -1$ mm and $\kappa_{2,2}(u) = 0$. Without loss of generality, the networks at the terminals of the wire pair are modeled by the lumped circuits shown in Fig. 8, with ground impedances Z_{G}, and series impedances $Z_{\mathrm{S1},X}$, $Z_{\mathrm{S2},X}$ are introduced as

$$Z_{\substack{\mathrm{S1},X \\ \mathrm{S2},X}} = Z_{\mathrm{D}}/2 \pm Z_{\delta} \tag{22}$$

where subscript $X = \mathrm{L}, \mathrm{R}$ denotes the left and right line-end, respectively, Z_{D} is the differential mode (DM) impedance of the wire pair, whereas the impedance Z_{δ} ($0 \leq Z_{\delta} < Z_{\mathrm{D}}/2$) accounts for possible imbalance w.r.t. ground affecting the terminal networks. Accordingly, the port constraints at the left (L) and right (R) ends are expressed by the impedance matrices

$$\mathbf{Z}_{\mathrm{L}} = \mathbf{Z}_{\mathrm{R}} = \begin{bmatrix} \frac{Z_{\mathrm{D}}}{2} - Z_{\delta} + Z_{\mathrm{G}} & Z_{\mathrm{G}} \\ Z_{\mathrm{G}} & \frac{Z_{\mathrm{D}}}{2} + Z_{\delta} + Z_{\mathrm{G}}. \end{bmatrix} \tag{23}$$

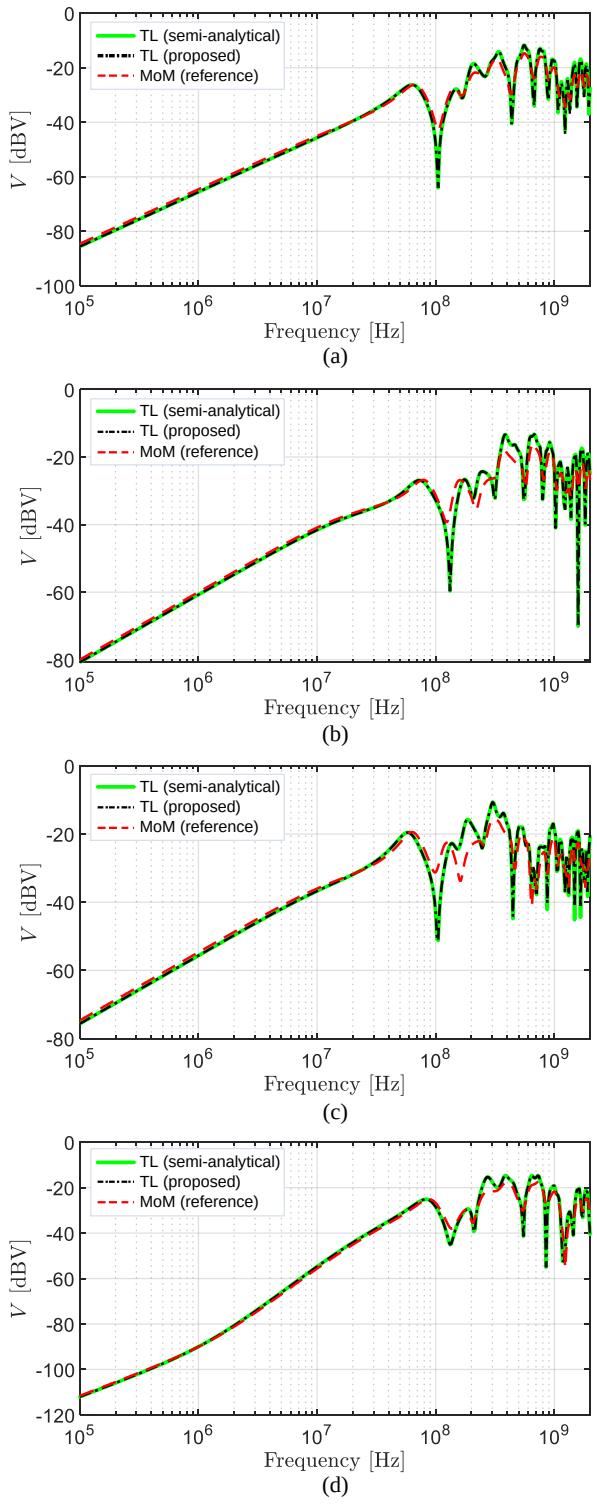

Fig. 7. Voltages induced at the right terminal of single-wire knots: (a) *Reference knot*. (b) *Tight knot*. (c) *Tall knot*. (d) *Small knot*.

To predict the modal voltages at the line ends, the similarity transformation matrices $\mathbf{T}_\mathrm{V}$ and $\mathbf{T}_\mathrm{I}$ are introduced, to relate physical voltages/currents at the left ($\mathbf{V}_\mathrm{L}, \mathbf{I}_\mathrm{L}$ in Fig. 2) and right ($\mathbf{V}_\mathrm{R}, \mathbf{I}_\mathrm{R}$ in Fig. 2) terminations with the corresponding common mode (CM) and DM quantities as

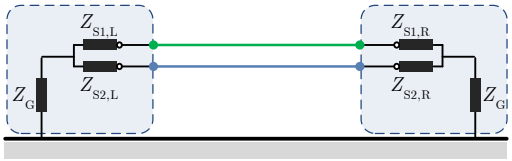

Fig. 8. Lumped-T networks at the terminals of the knotted wire pair.

$$\begin{bmatrix} V_{X,\mathrm{CM}} \\ V_{X,\mathrm{DM}} \end{bmatrix} = \mathbf{T}_\mathrm{V} \begin{bmatrix} V_{X,1} \\ V_{X,2} \end{bmatrix}, \quad \begin{bmatrix} I_{X,\mathrm{CM}} \\ I_{X,\mathrm{DM}} \end{bmatrix} = \mathbf{T}_\mathrm{I} \begin{bmatrix} I_{X,1} \\ I_{X,2} \end{bmatrix} \tag{24}$$

where

$$\mathbf{T}_\mathrm{V} = \begin{bmatrix} 1/2 & 1/2 \\ 1 & -1 \end{bmatrix}, \ \mathbf{T}_\mathrm{I} = \begin{bmatrix} 1 & 1 \\ 1/2 & -1/2 \end{bmatrix}. \tag{25}$$

For prediction of the induced CM voltages, the terminal networks are assumed to be balanced (i.e., $Z_\delta = 0$) and matched to the line DM impedance. To this end, the characteristic DM impedance of the knotted wire-pair was evaluated, and the obtained value was assigned to $Z_\mathrm{D} = 160\ \Omega$. Without loss of generality, in the simulation, the same value was assigned also to Z_G. The induced CM voltage (left end) evaluated by the proposed numerical RS model is compared versus MoM prediction in Fig. 9. The plots in the first panel were obtained for the *reference knot*, those in the second panel for the *tall knot*. The comparison substantially confirms the conclusions already drawn for previous examples. Namely, for both knot structures, the predictions obtained by the proposed method reproduce pretty well the outcome of MoM simulation, with discrepancies increasing in the hundreds of megahertz, where differences in the order of a few decibels start to be observed. As previously noted, model accuracy decreases as the vertical size of the knot increases (see *tall knot*), and consequently the dimension of the TL cross section is no longer negligible with respect to the wavelength.

Since the two wires in the knot are on average at the same height above ground, CM excitation is the dominant effect in field-to-wire coupling, and the induced DM noise is to be mainly ascribed to CM-to-DM conversion due to imbalance of the terminal sections [1]. Hence, for prediction of the induced DM voltages, a slight imbalance is introduced between the two series impedances, that is $Z_\delta = 5\ \Omega$. Meanwhile, the other impedances were assigned the values: $Z_\mathrm{G} = Z_\mathrm{D} = 160\ \Omega$. Predictions of the DM voltages induced at the left end of the knotted wire pairs under analysis are compared versus MoM simulation in Fig. 10. On the whole, the comparison confirms the effectiveness of the proposed method also for the prediction of the DM voltages, even if larger discrepancies w.r.t. MoM simulation are observed above 200 MHz approximately.

A small component of the DM current is directly induced by the external field in the terminal loads. In general, this component depends on the cross-sectional geometry of the two wires in the line, is very small, and therefore hard to predict due to high sensitivity to external effects such as scattered field, cable orientation, vertical risers, etc. The validation of the DM current previously discussed refers to

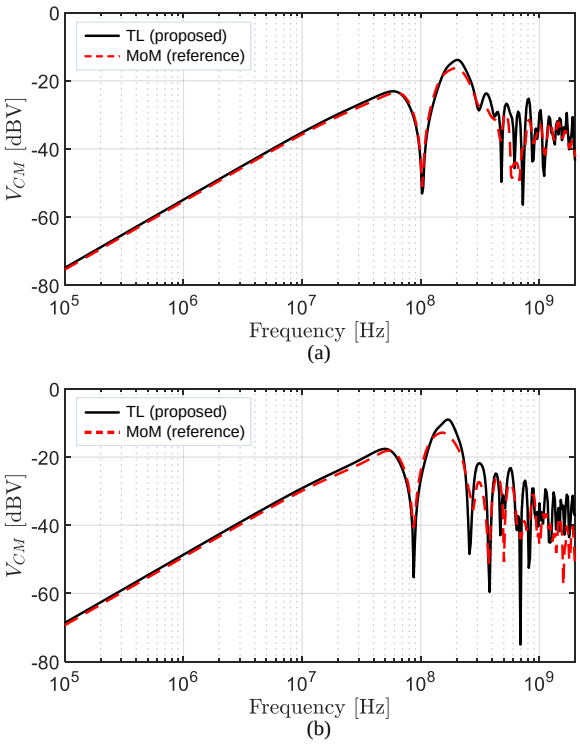

Fig. 9. Predictions of the CM voltage induced at the left terminal of the parallel-wire knots: (a) *reference* and (b) *tall knot*.

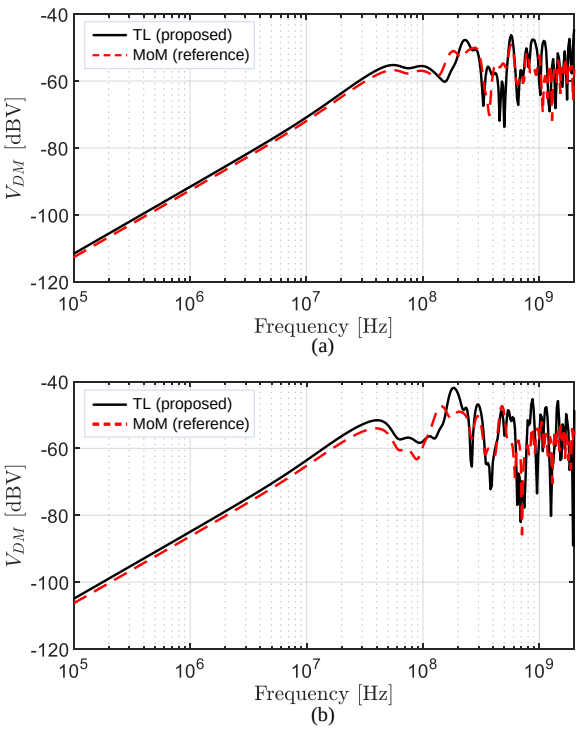

Fig. 10. Predictions of the DM voltage induced at the left terminal of the parallel-wire knots: (a) *reference* and (b) *tall knot*, with unbalanced configuration.

slightly imbalanced network configurations, where CM-to-DM conversion takes place at the line ends and represents the dominant contribution. That choice is motivated by the fact that in practical installations, loads are generally not perfectly balanced, and mode conversion in the load sections plays a crucial role in determining the susceptibility of differential pairs. In that case, the component of the DM current directly induced by the external field in the terminal loads and due to the cable structure cannot be validated as it represents a minor contribution. Prediction of such a "pure" DM current component (in a line configuration with balanced terminal networks) is provided in the following by computing the DM voltages induced across balanced loads, floating with respect to ground. This was done by considering the same knotted wire-pair structures (*reference knot* and *tall knot*), with impedances $Z_{\mathrm{D}} = 160\ \Omega$ (i.e., $Z_{\delta} = 0\ \Omega$) connected between the terminals of the two wires in the knot so to realize the balanced configuration (with floating terminations). To incorporate these changes, the terminal constrains at the knot ends were reformulated in terms of Norton equivalent representation, instead of the original Thevenin formulation, no longer possible in the case of terminations floating with respect to ground. Simulation of these new test cases yielded the results shown in Fig. 11.

As expected, the induced DM voltages are significantly smaller in magnitude with respect to the previous cases. This is especially true for the *reference knot* structure, which exhibits a decrease in the induced DM voltage from -112.3 dBV to -165.9 dBV at 100 kHz. For the tall knot, the induced DM voltage is larger than for the *reference knot*, due to increased coupling. In both cases, in spite of a few of discrepancies (more evident for the *tall* than for the *reference knot*), which have to be ascribed to structural characteristics of the wiring structure only instead of CM-to-DM conversion as in the previous examples, the proposed model yields predictions in satisfactory agreement with those obtained by full-wave simulation.

VI. Conclusion

In this work, a novel modelling framework has been proposed for computationally efficient prediction of field-to-wire coupling effects in arbitrarily oriented wiring harnesses. The proposed approach combines an accurate parametric representation of wire trajectories, here obtained by resorting to the Frenet frame, with an approximate TL-based numerical model for RS prediction. Likewise previous hybrid approaches in the literature [1], [3]–[5], the proposed numerical model does not necessarily require a continuous mathematical representation of wire trajectories and field distribution along the bundle length, but their knowledge at discrete points along the cable path only. With respect to those models, however, its applicability is not limited to bundles approximately parallel to ground, since the simplifying assumptions usually exploited by those models are here removed. Accuracy and computational efficiency of the proposed model have been investigated by comparison versus full-wave (MoM) simulation of two wiring structures exhibiting strong nonuniformity with respect to ground, which is a parabola-shaped and a trefoil knot-shaped line above ground. For the sake of completeness, simulations were also carried out by exploiting an exact semianalytical TL

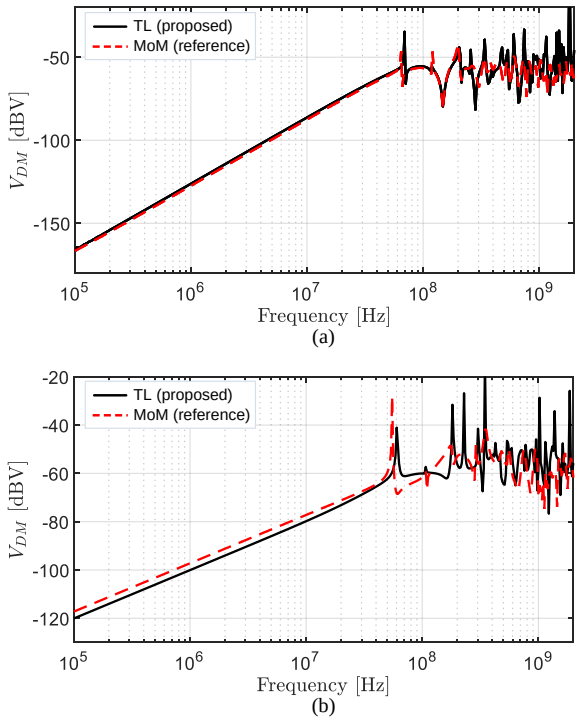

Fig. 11. Predictions of the DM voltage induced at the left terminal of the parallel-wire knots: (a) *reference* and (b) *tall knot*, with terminal sections floating with respect to ground (balanced configuration).

model, whose predictions are taken as reference, since they provide information on the maximum accuracy achievable by TL-based modelling.

In terms of accuracy, the comparison proves that the proposed model, although approximate, retains the same accuracy as the exact TL-based solution. Also, the comparison with MoM simulation confirms that TL-based approaches represent effective alternatives to full-wave simulation in a wide frequency range, even for strongly nonuniform wiring structures where basic assumptions of TL theory are violated or partially satisfied. The comparison in terms of simulation times indicates that the proposed numerical approach assures a significant speed-up not only with respect to full-wave simulation, but also with respect to the exact semianalytical solution scheme, whose computational burden becomes even more prohibitive than full-wave simulation for complex geometries, such as the knot-shape wiring here considered.

Eventually, it is worth pointing out that although the examples presented in this work are limited to single wires or wire-pairs only, the proposed methodology can be readily combined with the one introduced in [5] to obtain a computationally efficient tool for the prediction of RS in complex wiring harnesses, involving several wires (or twisted-wire pairs) and not only exhibiting arbitrarily shaped routing but also random movements of the wires along the cable length.

REFERENCES

[1] G. Spadacini, F. Grassi, F. Marliani, and S. A. Pignari, "Transmission-line model for field-to-wire coupling in bundles of twisted-wire pairs above ground," *IEEE Trans. Electromagn. Compat.*, vol. 56, no. 6, pp. 1682–1690, 2014.

[2] M. Brignone, F. Delfino, R. Procopio, M. Rossi, F. Rachidi, and S. V. Tkachenko, "An effective approach for high-frequency electromagnetic field-to-line coupling analysis based on regularization techniques," *IEEE Trans. Electromagn. Compat.*, vol. 54, no. 6, pp. 1289–1297, 2012.

[3] G. Spadacini, F. Grassi, and S. A. Pignari, "Field-to-wire coupling model for the common mode in random bundles of twisted-wire pairs," *IEEE Trans. Electromagn. Compat.*, vol. 57, no. 5, pp. 1246–1254, 2015.

[4] O. Gassab and W.-Y. Yin, "Characterization of electromagnetic wave coupling with a twisted bundle of twisted wire pairs (TBTWPs) above a ground plane," *IEEE Trans. Electromagn. Compat.*, vol. 61, no. 1, pp. 251–260, 2018.

[5] X. Liu, F. Grassi, G. Spadacini, and S. A. Pignari, "Physically based modeling of hand-assembled wire bundles for accurate EMC prediction," *IEEE Trans. Electromagn. Compat.*, vol. 62, no. 3, pp. 914–922, 2020.

[6] C. R. Paul, *Analysis of multiconductor transmission lines*. John Wiley & Sons, 2008.

[7] H. Haase, T. Steinmetz, and J. Nitsch, "New propagation models for electromagnetic waves along uniform and nonuniform cables," *IEEE Trans. Electromagn. Compat.*, vol. 46, no. 3, pp. 345–352, 2004.

[8] H. Haase, J. Nitsch, and T. Steinmetz, "Transmission-line super theory: A new approach to an effective calculation of electromagnetic interactions," *URSI Radio Sci. Bull.*, vol. 2003, no. 307, pp. 33–60, 2003.

[9] X. Song, D. Su, J. Wang, and B. Li, "Field-to-wire coupling model for wire bundles with strongly non-uniform path," in *Proc. Int. Appl. Comput. Electromagn. Soc. Symp.-China (ACES)*, 2018, pp. 1–2.

[10] F. Klok, "Two moving coordinate frames for sweeping along a 3D trajectory," *Comput. Aided Geom. Des.*, vol. 3, no. 3, pp. 217–229, 1986.

[11] A. K. Agrawal, H. J. Price, and S. H. Gurbaxani, "Transient response of multiconductor transmission lines excited by a nonuniform electromagnetic field," *IEEE Trans. Electromagn. Compat.*, no. 2, pp. 119–129, 1980.

[12] G. Spadacini, S. A. Pignari, and F. Marliani, "Closed-form transmission line model for radiated susceptibility in metallic enclosures," *IEEE Trans. Electromagn. Compat.*, vol. 47, no. 4, pp. 701–708, 2005.

[13] S. A. Pignari and G. Spadacini, "Plane-wave coupling to a twisted-wire pair above ground," *IEEE Trans. Electromagn. Compat.*, vol. 53, no. 2, pp. 508–523, 2011.

[14] S. A. Pignari and D. Bellan, "Incorporating vertical risers in the transmission line equations with external sources," in *Proc. Int. Symp. Electromagn. Compat.*, vol. 3, Aug. 2004, pp. 974–979.

[15] O. Gassab, L. Zhou, Z. Zhao, and W. Yin, "Effect of the Scattered Field on the Terminal Risers in Twisted-Wire Pairs With Floating Loads," *IEEE Trans. Electromagn. Compat.*, vol. 62, no. 1, pp. 291–295, 2020.

[16] J. C. Clements, C. R. Paul, and A. T. Adams, "Computation of the capacitance matrix for systems of dielectric-coated cylindrical conductors," *IEEE Trans. Electromagn. Compat.*, no. 4, pp. 238–248, 1975.

[17] C. J. Alberto *et al.*, *Physical And Numerical Models In Knot Theory: Including Applications To The Life Sciences*. World Scientific, 2005.

[18] A. R. Shastri, "Polynomial representations of knots," *Tohoku Math. J. Second Ser.*, vol. 44, no. 1, pp. 11–17, 1992.